Available online at www.sciencedirect.com

ScienceDirect

journal homepage: www.elsevier.com/locate/he

Sustainable hydrogen production by CdO/exfoliated g-C_3N_4 via photoreforming of formaldehyde containing wastewater

Thurga Devi Munusamy [a], *Sim Yee Chin* [a,b], *Mostafa Tarek* [a], *Md.Maksudur Rahman Khan* [a,b,*]

[a] *Department of Chemical Engineering, College of Engineering, Universiti Malaysia Pahang, 26300 Gambang, Pahang, Malaysia*

[b] *Centre of Excellence for Advanced Research in Fluid Flow (CARIFF), Universiti Malaysia Pahang, 26300, Gambang, Pahang, Malaysia*

HIGHLIGHTS

- Exfoliated g-C_3N_4 nanosheets were successfully prepared via chemical treatment.
- The newly formulated CdO/exfoliated g-C_3N_4 enhance hydrogen production.
- Treatment of synthetic wastewater through photoreforming of aqueous formaldehyde.
- Dual role of organic compounds as hole scavengers and proton donor.
- Organic oxidation and hydrogen generation by Z-Scheme reaction mechanism.

GRAPHICAL ABSTRACT

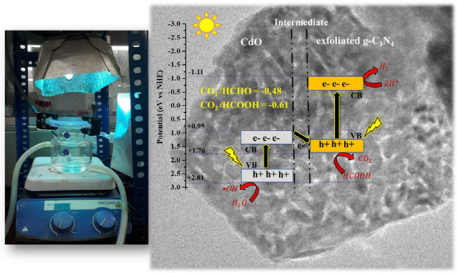

ARTICLE INFO

Article history:
Received 19 September 2020
Received in revised form
2 January 2021
Accepted 26 January 2021
Available online xxx

Keywords:
Photoreforming
Hydrogen

ABSTRACT

Graphitic carbon nitride (g-C_3N_4) has been well-known as an appealing semiconducting material for photocatalytic hydrogen production despite its restricted active sites and poor electronic properties. In this work, exfoliated g-C_3N_4 nanosheets were synthesised by chemical treatment of the bulk graphitic carbon nitride (gCN) and the nanosheets were further doped with CdO. The photocatalysts produced were extensively characterized by diverse analysis including XRD, BET, XPS, TEM, FESEM, UV-Vis spectroscopy and PL analysis. The BET surface area of CdO/exfoliated g-C_3N_4, 40.1 m^2 g^{-1} was doubled in comparison to the exfoliated g-C_3N_4. Numerous electrochemical analyses such as Mott-Schottky, linear weep voltammetry and chronoamperometry were also performed in a standard photoelectrochemical system with three-electrode cell. The hydrothermally synthesised CdO/

* Corresponding author. Department of Chemical Engineering, College of Engineering, Universiti Malaysia Pahang, 26300 Gambang, Pahang, Malaysia.
E-mail address: mrkhancep@yahoo.com (Md.MaksudurR. Khan).

https://doi.org/10.1016/j.ijhydene.2021.01.176

Please cite this article as: Munusamy TD et al., Sustainable hydrogen production by CdO/exfoliated g-C_3N_4 via photoreforming of formaldehyde containing wastewater, International Journal of Hydrogen Energy, https://doi.org/10.1016/j.ijhydene.2021.01.176

Wastewater
Formaldehyde
Z-Scheme

exfoliated g-C_3N_4 resulted higher amount of hydrogen evolution (145 μmol/g) for the photoreforming of aqueous formaldehyde than the CdO (20 μmol/g), bulk gCN (58 μmol/g) and exfoliated g-C_3N_4 (87 μmol/g). The excellent hydrogen production rate using CdO/exfoliated g-C_3N_4 nanocomposite could be ascribed by higher number of active sites as well as shorter path of the charge carries to the reaction surface. The anticipated Z-Scheme mechanism has demonstrated a synergistic impact between the CdO and exfoliated g-C_3N_4 where the organic compounds acting as hole scavenger as well as contribute protons, H^+ for the effective hydrogen production. Thus, it is clearly confirmed that the newly formulated CdO/exfoliated g-C_3N_4 has an outstanding potentiality for environmental remediation and conversion sectors.

Introduction

Globally, hydrogen demand has grown beyond threefold since 1975 and continue to accelerate by time. According to International Energy Agency (IEA), the largest source of hydrogen production, natural gas is accounting about three quarters of annual global hydrogen production (70 million tonnes). However, the hydrogen production by conventional approach is emitting carbon dioxide, CO_2 up to 830 million tonnes [1]. In this case, a more cost-effective technology to produce renewable and sustainable hydrogen is in need. Thereby, photoreforming of hydrogen production has gained great attention owing to the multiple benefits. Photoreforming process does not require additional energy than solar energy, can be carried out in a small-grid system as well as capable to generate pure fuel-cell grade hydrogen [2]. The technique comes with a combination of reduction of water and oxidation of organic compounds in a single process. In the conduction band (CB), the electron is excited by the photon energy and hence reducing the water to hydrogen, whereas at valence band (VB), the photo-induced holes aids in oxidizing the organic compounds. Therefore, the technology represents a suitable candidate for simultaneous energy production and wastewater treatment. The general water splitting and photoreforming reactions are presented in equations (1) and (2) respectively [3]:

$$H_2O \rightarrow H_2 + \tfrac{1}{2}O_2 \quad (1)$$

$$C_xH_yO_z + (2n-y)H_2O \rightarrow nCO_2 + (2n-y+x/2)H_2 \quad (2)$$

As a substitute of organic compounds, organic pollutants in wastewater could act as electron donor and aid the dual process of water treatment and hydrogen production [4]. Specifically, the wastewaters from petrochemical industries contain substantial amount of organic pollutants such as benzenes, aldehydes and phenols with high toxicity and are naturally less biodegradable [5,6]. Concurrently, the major constituent of petrochemical wastewater, formaldehyde (FA) generates contaminated effluents of FA concentration ranging from 100 to 10000 ppm [7]. As well known, this enormously toxic wastewater has plethora of harmful effects towards human as well aquatic ecosystem. According to International Agency for Research on Cancer (IARC), formaldehyde is carcinogenic to humans [8]. Hence, it is utmost important to treat the petrochemical wastewaters in an economically feasible and environmentally friendly process before discharging into the water bodies.

Graphitic carbon nitride, g-C_3N_4 is an abundantly available, chemically stable, convenient to synthesise and low-cost materials that was widely explored for hydrogen production [9,10]. Nevertheless, the bulk g-C_3N_4 endures poor visible light absorption, restricted surface area and also rapid electron-hole pairs' recombination which consequently limit the photo-reactions [10,11]. Guo et al. investigated the activity of pure g-C_3N_4 that acted as electron donor in photoreforming the aqueous methanol and found that only 6 μmol g^{-1} h^{-1} hydrogen was evolved for a duration of 3 h [12]. Li et al., explored the similar photocatalytic reaction for 2 h using triethanolamine as sacrificial agent and observed minimal hydrogen evolution rate (1.9 μmol g^{-1} h^{-1}) by employing bulk g-C_3N_4 as the catalyst [13]. Wu and co-workers synthesised g-C_3N_4 nanosheets by repeated calcination of bulk g-C_3N_4 and the authors claimed that the BET surface area was tremendously enlarged in the g-C_3N_4 nanosheets (60.5 m^2 g^{-1}) than the bulk g-C_3N_4 (9.1 m^2 g^{-1}) [14]. Literatures have confirmed that ultrathin nanosheets have large surface area and shortened the path between charge carriers relative to the bulk g-C_3N_4 [15,16]. Hence, exfoliation is the preeminent one among the ultimate methods to convert the delamination of bulk g-C_3N_4 into free standing nanosheets. Nevertheless, the band gap of nanosheets are usually higher due to quantum confinement effect therefore doping with narrow band gap semiconductor are crucial to achieve optimum photocatalytic activity [17]. Commonly, noble metals were employed in photocatalytic reactions such as Au, Ag, Pt, Ru and many more as a co-catalyst [18–20]. Although noble metals-derived catalysts exhibit excellent activities, their utilization are limited because these materials are not cost effective. Besides, transition metal dichalcogenides (TMDs) showing great performance for HER activity mainly the metal sulphides are highly conductive, broadly available and cost-effective. However, poor stabilities becoming a limitation for their feasible applications [21,22]. Therefore, taking into consideration the above limitations, metal oxide based dopant is given attention. In such circumstances, doping with cadmium oxide (CdO) could be a splendid strategy due to its appropriate band gap as well

Please cite this article as: Munusamy TD et al., Sustainable hydrogen production by CdO/exfoliated g-C_3N_4 via photoreforming of formaldehyde containing wastewater, International Journal of Hydrogen Energy, https://doi.org/10.1016/j.ijhydene.2021.01.176

as extraordinary chemical, electrical and optical properties [23,24].

Conventionally, photoreforming were performed by various biomass-derived oxygenates including methanol, ethanol or glycerol which act as readily transportable hydrogen carriers [25]. Meanwhile, the study on converting wastes into useful energy sources through photoreforming reaction could be very interesting. The photocatalytic reforming of hydrogen production from aqueous formaldehyde is more appealing because it can also be considered as a cleaner technology in treating this harmful petrochemical wastewater effluent. Up to date, only limited studies were performed. During our previous work, we demonstrated the preparation of hybrid g-C_3N_4/CdO nanocomposite by self-assembly method where the study was limited to dye degradation activities [26]. Despite the advantages of bulk g-C_3N_4, this amorphous material possesses not only low surface area but also quick recombination rate of charge carriers. Therefore, the attentions of current work were given to the fabrication of exfoliated g-C_3N_4 by chemical treatment and this material was further doped with CdO by hydrothermal method. As per our knowledge, we demonstrated a novel approach on the formulation of CdO/exfoliated g-C_3N_4 nanocomposite. The physico-chemical attributes of the catalysts were examined by BET, XRD, TEM, XPS, UV-Vis spectroscopy and PL analysis. The band edges of the catalyst were evaluated by Mott-Schottky analysis. Electrochemical characterization of the catalysts under dark and light illumination were performed by linear sweep voltammetry (LSV) and chronoamperometry. Photoreforming reaction of the synthetic petrochemical wastewater, an aqueous solution of formaldehyde, was conducted to evaluate the catalysts' performance for hydrogen production. A plausible Z-Scheme mechanism was subsequently elucidated.

Experimental section

Materials

Melamine [$C_3H_6N_6$], cadmium nitrate tetrahydrate [$Cd(NO_3)_2.4H_2O$], sodium bicarbonate [$NaHCO_3$], formaldehyde (FA), agar and Nafion solution (5 wt%) were acquired from Sigma Aldrich, Malaysia while sulphuric acid [H_2SO_4 98%], isopropanol [C_3H_8O 96%] and ethanol [C_2H_5OH 99%] were obtained from HmbG, Malaysia.

Preparation of exfoliated g-C_3N_4

Bulk g-C_3N_4 was synthesised by thermal polycondensation technique as reported by Papailias et al., [27]. Specifically, 4 g of melamine was calcined at 650 °C with a ramping rate of 5 °C/min where the resulting solid was labelled as bulk gCN. The exfoliated g-C_3N_4 was synthesised by chemical exfoliation technique. The as-prepared bulk gCN (0.5 g) was added into H_2SO_4 (8 mL). Then, DI water (2 mL) was gently added while stirring for another 1 h at room temperature. It was carefully handled during this step since heat dissipated due to exothermic reactions. Thereafter, the suspension was washed with DI water for several times. The precipitate obtained was re-disperse into 30 mL of isopropanol and this mixture was subjected to ultrasonication for another 2 h. Next, the liquid was decanted and dried overnight at 80 °C. Lastly, the solid sample was ground into fine powders and named as exfoliated g-C_3N_4.

Synthesis of CdO/exfoliated g-C_3N_4

The CdO/exfoliated g-C_3N_4 was formulated by using chemical precipitation of CdO and hydrothermal methods [28]. In detail, certain amount of as-prepared exfoliated g-C_3N_4 and 0.1 M of cadmium nitrate salt was introduced into DI water (30 mL). The mass ratio of exfoliated g-C_3N_4 to CdO was fixed at 5:1 in reference to Deng et al., who proved that where, 20 wt% was showed the best performance for the prepared catalyst [29]. In the chemical precipitation step, 1 M of NaOH was added slowly into the mixture to form CdO nanoparticles. The mixture was retained at pH 8 and stirred for 1 h at 60 °C. Afterward, the suspension was autoclaved at 140 °C for 8 h by utilizing Teflon-lined hydrothermal reactor. The reactor was left to room temperature and the suspension was washed with DI water and ethanol to eliminate any impurities. Lastly, the solid was dried (80 °C) overnight and the brownish-yellow powder gained was labelled as CdO/exfoliated g-C_3N_4. The detailed characterization techniques of the as-prepared photocatalysts were discussed in the supplementary information.

Electrode preparation

The electrode was designed by ink-brushing technique by referring to Rezaul et al., [30]. In detailed, the as-prepared photocatalyst (25 mg) was mixed with Nafion (80 μL) and isopropanol (140 μL) prior to the ultrasonication for 4 h. The ink formed was thoroughly brushed in Toray carbon paper (1 cm × 1 cm) and allowed to dry completely.

Electrochemical analysis

The electrochemical characterization was performed by employing dual chamber of photoelectrochemical cell (PEC) associated with a potentiostat (Autolab Compact PGSTAT204, Netherland) and the light source used was Xenon 300 high brightness cold light. The anodic and cathodic region of the chambers were isolated by Nafion 117 membrane. The three-electrode system employing $NaHCO_3$ (0.1 M) as electrolyte, was constituted of Ag/AgCl electrode (reference electrode), platinum foil (counter electrode) and CdO/exfoliated g-C_3N_4 (working electrode). Prior to start the analysis, N_2 gas was purged into the aqueous solution of the electrolyte for 30 min at a constant flow rate thereby removing dissolved oxygen in the system. Mott-Schottky analysis was executed at a fixed voltage of 0 V with a frequency of 500 Hz. Linear sweep voltammetry (LSV) was performed at an ambient condition under light irradiation with a potential ranging from +0.2 to −1.0 V vs. NHE and scan rate of 10 mV/s. Additionally, the light sensitivity of the photocatalysts was examined by chronoamperometry test driven at 0 V under both light off and light on conditions.

Please cite this article as: Munusamy TD et al., Sustainable hydrogen production by CdO/exfoliated g-C_3N_4 via photoreforming of formaldehyde containing wastewater, International Journal of Hydrogen Energy, https://doi.org/10.1016/j.ijhydene.2021.01.176

Photoreforming activity

Photoreforming activity was accomplished in a 200 mL quartz reactor where the openings of the glass were sealed with a glass lid and silicon capping. A 100 W Xenon lamp was employed where it was kept vertically with a length of 15 cm from the reactant solution. The intensity of the light was measured by the photometer and observed to be 75 W/m^2. The photoreactor set-up employed in this study are illustrated in Fig. S1. Practically, catalyst (50 mg) was dispersed in 100 mL of 100 mg/L formaldehyde (petrochemical wastewater constituent) in all the experiments. Before the reaction commenced, the dissolved oxygen and air in the reactor was displaced by purging N_2 gas for 30 min. A constant stirring was given by placing magnetic stirrer to avoid sedimentation of photocatalysts while maintaining the system at an ambient condition. The hydrogen (H_2) gas generated was collected into Tedlar gas sampling bags and analyzed by gas chromatography (GC-TCD). Photoreforming reaction was monitored for a total duration of eight hour and the cumulative hydrogen generated were quantified. In this case, the experiments were run in triplicate and error bars were adopted to indicate the standard deviation.

Results and discussions

XRD and BET analysis

The Brunauer-Emmett-Teller (BET) surface area of the photocatalysts was evaluated and respective N_2 adsorption-desorption isotherm was plotted in Fig. 1(a). The exfoliated g-C_3N_4 and CdO/exfoliated g-C_3N_4 exhibited type IV isotherm with H3 and H4 hysteresis loops respectively, verifying the occurrence of narrow silt-like mesopores in the CdO/exfoliated g-C_3N_4 due to materials stacking and the wide gap of the loop indicated the presence of irregular shapes of particles with internal voids [31]. The bulk gCN possessed a surface area of 6.3 m^2g^{-1}. Generally, pure g-C_3N_4 contained poor surface area and Wu et al., also demonstrated that the specific surface area of bulk g-C_3N_4 was as low as 2.88 m^2 g^{-1} [32]. Meanwhile, the surface area of exfoliated g-C_3N_4 was 22.8 m^2g^{-1} whereas CdO/exfoliated g-C_3N_4 possessed approximately two times larger surface area (46.1 m^2g^{-1}). This was evidenced from the effect of formation of pores on the surface of composite catalyst could contribute to the enlargement of the area [33]. The pore size distribution of the nanocomposite as presented in Inset Fig. 1(a) revealed that the pore size was within the range (3–25 nm) and confirmed the presence of mesopores. Thus, large surface area of CdO/exfoliated g-C_3N_4 could provide more active sites for the adsorption of organic pollutants leading to higher photocatalytic performance.

The XRD pattern of the prepared catalyst are illustrated in Fig. 1(b). For the bulk gCN and exfoliated g-C_3N_4 two distinct peaks (DB card 9000046) were obtained. The first peak was positioned at 13.2° (110) represented the in-planar tri-s-triazine units whereas the second peak was at 28.1° (002) which revealed the interaction of interlayer stacking in conjugated aromatic system that commonly found in graphitic materials. However, it was observed that the peak at 12.6° in exfoliated became weaker as compared to bulk gCN owing to decline in the planar size after exfoliation [34]. Based on the CdO/exfoliated g-C_3N_4 pattern, a total seven diffraction peaks were observed and among them five Bragg peaks that located at 33.2°(111), 38.4°(200), 55.3°(220), 65.9°(311) and 69.1°(222) corresponded to monteponite (DB card 1011003) phase of CdO. The crystalline size of the CdO at plane (111) was calculated by applying the Debye Scherrer's equation as demonstrated in the supplementary, Equation S1 and found to be 14.6 nm in which the value was in line with reported literature [35]. The other two peaks were related to g-C_3N_4 phase and holds similar plane positions as discussed above. Hence, these outcomes proved the successful formation of CdO/exfoliated g-C_3N_4 nanocomposite.

Morphological analysis

The morphological analysis of the synthesised photocatalysts was examined by TEM as demonstrated in Fig. 2. The image in Fig. 2(a) reveals the ultrathin characteristics of the exfoliated g-C_3N_4. Meanwhile, the bulk gCN exhibited lamellar structure with crimpled edges as can be observed in the Inset of Fig. 2(a). The decorated CdO onto the exfoliated g-C_3N_4 nanosheets are illustrated Fig. 2(b) and zoomed area is further illustrated in Inset of Fig. 2(b). It was denoted that the exfoliated g-C_3N_4 exhibited some interlayers due to irregular arrangement of the nanosheets creating the pores [36]. Alongside, the spherical-shaped CdO nanoparticles were uniformly aggregated resulting the formation of homogeneous distribution. The diameter of the CdO was approximately 15 nm and the value are in accordance with the crystal size of CdO obtained from the XRD result. Hence, TEM analysis confirmed that the CdO components was firmly anchored on the nanosheets and hence enhancing the composite's surface area where the result was also supported by BET analysis. To further verify the successful fabrication of CdO/exfoliated g-C_3N_4, elemental mapping was examined for the nanocomposite. Based on Fig. 2(c–f), it can be deduced that elements Cd and O were uniformly distributed on the exfoliated g-C_3N_4 nanosheets.

The electronic state and chemical composition of CdO/exfoliated g-C_3N_4 was evaluated by XPS analysis. All the dominant peaks of cadmium, oxygen, carbon and nitrogen present in the nanocomposite. The doublet peaks of $Cd3d_{5/2}$ and $Cd3d_{3/2}$ in Fig. 3(a) positioned at 403.8 eV and 410.6 eV were corresponding to Cd^{2+} atoms [37]. Fig. 3(b) revealed that O1s peaks at 530.4 eV was attributed to the presence of O^{2-} [38]. From Fig. 3(c), the peaks of C1s was fitted into 286.6 eV that demonstrate the C-C of the surface adventitious carbon. Meanwhile, the peak positioned at 288.2 eV was ascribed to sp^2 hybridized carbon present in the aromatic ring (N–C=C). Based on Fig. 3(d), the N1s was deconvoluted into three peaks that possessed binding energies of 397.2, 398.6 and 399.7 eV. The peak at 397.2 eV represented the sp^2 bonded atoms from the triazine rings. Meanwhile, the peaks at 398.6 and 399.7 eV were contributed by bridging N atoms in tertiary nitrogen N-$(C)_3$ and C-N-H of the amino groups with hydrogen atom respectively [39,40]. Hence, the XPS analysis confirmed the association of CdO with exfoliated g-C_3N_4.

Please cite this article as: Munusamy TD et al., Sustainable hydrogen production by CdO/exfoliated g-C_3N_4 via photoreforming of formaldehyde containing wastewater, International Journal of Hydrogen Energy, https://doi.org/10.1016/j.ijhydene.2021.01.176

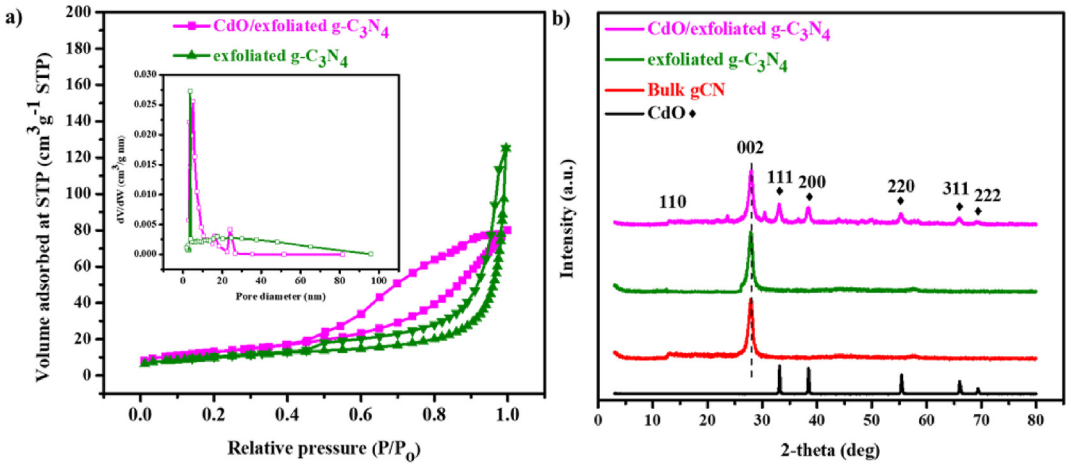

Fig. 1 – (a) N_2 adsorption-desorption isotherm [Inset: Pore size distribution], (b) XRD profile of exfoliated g-C_3N_4 and CdO/exfoliated g-C_3N_4.

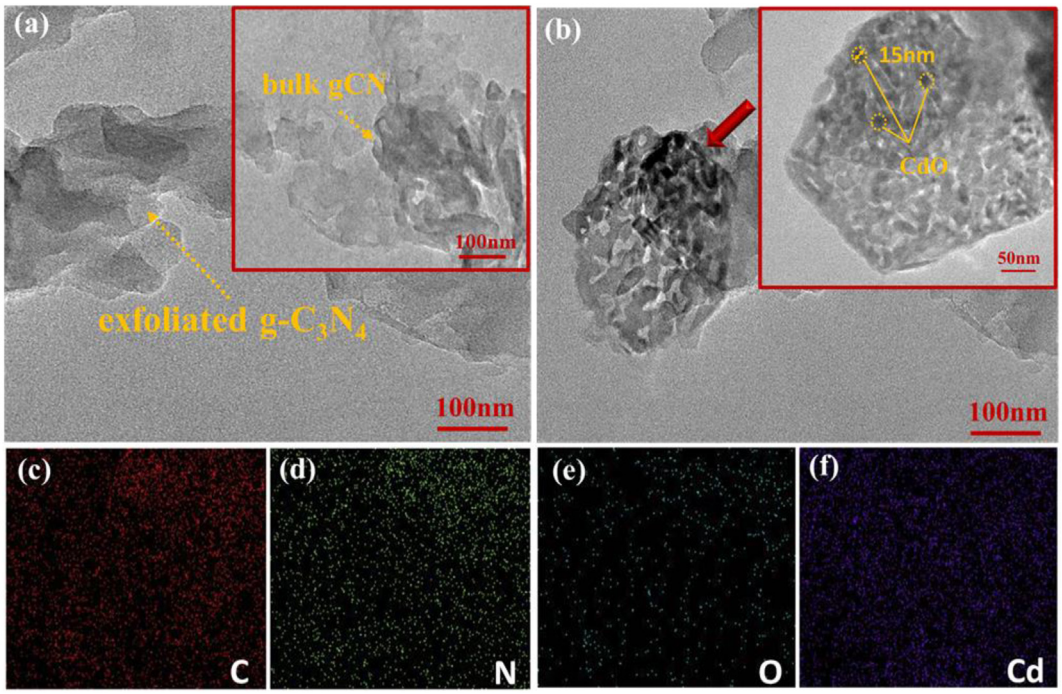

Fig. 2 – (a) TEM image of exfoliated g-C_3N_4 nanocomposite [Inset: TEM of bulk gCN], (b) TEM image of CdO/exfoliated g-C_3N_4 [Inset: TEM of CdO/exfoliated g-C_3N_4 zoomed at 50 nm], (c–f) EDX mapping of CdO/exfoliated g-C_3N_4.

Optical analysis

Absorption spectrum is one of the crucial analysis to examine the optical effects of the photocatalyst. The UV-Vis absorption spectrum of the CdO, exfoliated g-C_3N_4, and CdO/exfoliated g-C_3N_4 are presented in Fig. 4(a). A typical absorption band at approximately 325–400 nm was observed for exfoliated g-C_3N_4. As for CdO doped exfoliated g-C_3N_4, the absorption band was slightly red-shifted relative to pure exfoliated g-C_3N_4 indicating excellent photo-absorption in the visible region of the nanocomposite. The band gap was derived from Kubelka-Munk model as depicted in the supplementary, Equation S2. The band energy values were acquired by linearly extrapolating ($\alpha h\upsilon^{1/2}$) up to x-axis (Fig. 4(b)). As a result, the Tauc plot presented the band gap of CdO, exfoliated g-C_3N_4 and CdO/exfoliated g-C_3N_4 of 1.86, 2.87 and 2.23 eV respectively. In this regard, the addition of CdO could confine the band gap of the nanocomposite due to ability of Cd atoms to extend the л-electron conjugated of exfoliated g-C_3N_4 layer [41]. The impact on charge carrier migration was investigated by photoluminescence under light excitation of 385 nm and are illustrated in Fig. 4(b). It was noticeable that the bulk gCN possessed peak centered at 594 nm while exfoliated g-C_3N_4 has a PL band at 598 nm where the intensity was reduced implying the reduction in recombination rate of e-/h + pairs.

Please cite this article as: Munusamy TD et al., Sustainable hydrogen production by CdO/exfoliated g-C_3N_4 via photoreforming of formaldehyde containing wastewater, International Journal of Hydrogen Energy, https://doi.org/10.1016/j.ijhydene.2021.01.176

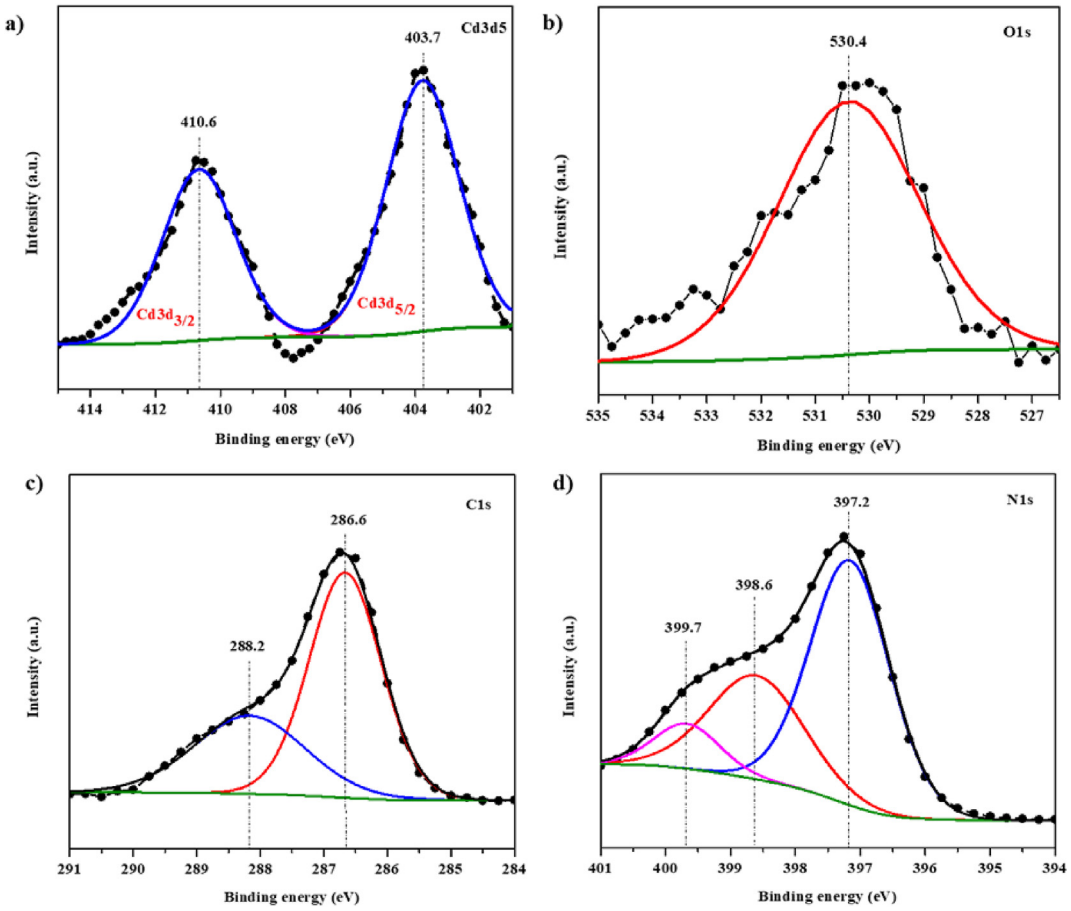

Fig. 3 – XPS spectra of CdO/exfoliated g-C_3N_4: (a) Cd3d5, (b) O1s, (c) C1s and (d) N1s.

The CdO/exfoliated g-C_3N_4 was greatly red-shifted (742 nm) due to lower band gap of the nanocomposite causing the emission of lower-energy photons with longer wavelength during the recombination of electrons with holes [42]. Accordingly, the intensity of CdO/exfoliated g-C_3N_4 was tremendously decreased revealing that CdO and exfoliated g-C_3N_4 could efficiently migrate the charges and inhibit the recombination rate resulting in higher photocatalytic performance of the nanocomposite [43].

Photoelectrochemical (PEC) test

The Mott-Schottky test was used to evaluate the band alignment, semiconductor type and the charge transfer process.

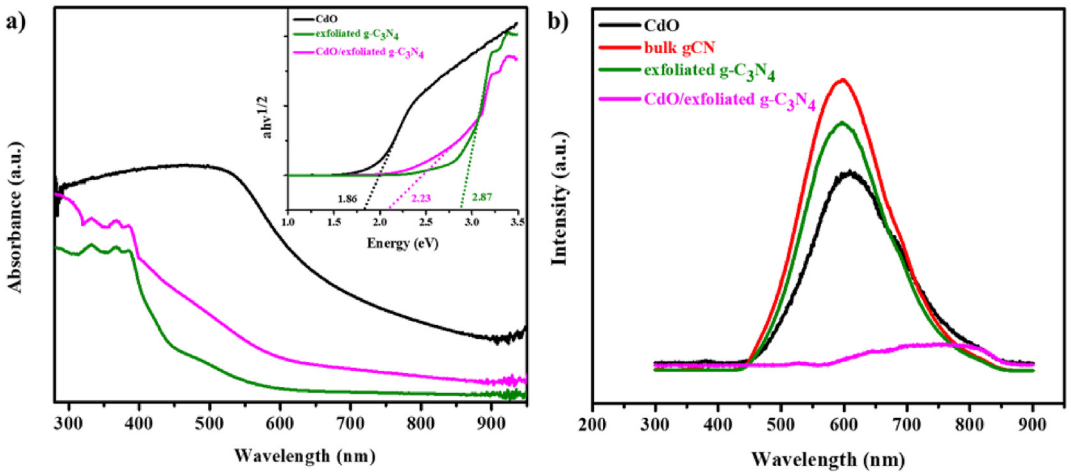

Fig. 4 – (a) UV-Vis absorption spectrum of CdO, exfoliated g-C_3N_4 and CdO/exfoliated g-C_3N_4 [Inset: Tauc plot of the photocatalysts], (b) PL spectrum at an excitation wavelength of 385 nm.

Please cite this article as: Munusamy TD et al., Sustainable hydrogen production by CdO/exfoliated g-C_3N_4 via photoreforming of formaldehyde containing wastewater, International Journal of Hydrogen Energy, https://doi.org/10.1016/j.ijhydene.2021.01.176

The analysis was conducted at potential 0 V with a frequency of 500 Hz under dark conditions. The flat band potentials (E_{fb}) of the photocatalysts were measured by performing Mott-Schottky test and can be referred from the extrapolated x-axis of the plot in Fig. 5. Therefore, the E_{fb} of CdO and exfoliated g-C_3N_4 were observed to be +0.54 and −1.72 eV (vs. NHE) respectively. Both the slopes were positive and indicates the intrinsic n-type properties of the semiconducting materials [44]. In this case, as the n-type material, the conduction band (CB) is located near the E_{fb} and were corrected according to the conversion formula, where E(NHE) is the corrected potential [45];

$$E(NHE) = E_{fb} + 0.059pH \quad (4)$$

Therefore, the CB of the as-prepared catalysts are as follows; CdO = +0.95 and exfoliated g-C_3N_4 = −1.11 (vs. NHE, pH = 7) after the pH correction and the values were close as reported in previous literatures [46,47]. In reference to the band gap energy (Tauc plot), the valence band (VB) were calculated based on equation (5) and the results obtained were as follows, CdO = +2.81 and exfoliated g-C_3N_4 = +1.76 (vs. NHE, pH = 7).

$$E_{VB} = E_{CB} + E_g \quad (5)$$

where E_{VB} is the valence band, E_{CB} is the conduction band and E_g is the band gap energy respectively.

LSV curves were plotted in the range of +0.2 V to −1.0 V vs. NHE with light illumination. Based on Fig. 6(a), the onset potential of CdO/exfoliated g-C_3N_4 shifted from −0.2 V to −1 V with an improve in the photocurrent density up to −0.85 mA/cm^2. Meanwhile, the reducing current of exfoliated g-C_3N_4 was only −0.26 mA/cm^2 at the similar applied potential. Thus, the result demonstrates that the integration of CdO could enhance the electron-hole separation and migration potentiality, consequently it could promote the photocatalytic reduction of protons to hydrogen, H_2 [48]. This outcome was also in accordance with PL results and reaffirmed that CdO/exfoliated g-C_3N_4 nanocomposite has the ability to restrict the charge carriers' recombination.

To further verify the photocurrent generation, chronoamperometry test was performed and the characteristic curve are presented in Fig. 6(b). Applied potential, 0 V was employed by alternating dark and under illumination conditions. As such instance, the cathodic current was noticed for all the prepared photocatalysts whereby the current was intensified in the light on conditions. It was clearly seen that the photocurrent responses appeared for both electrodes immediately when the light was emitted, however it promptly approached zero at the moment the light was cut off. In this case, the photocurrent value of the CdO/exfoliated g-C_3N_4 electrode was approximately three-fold larger than the exfoliated g-C_3N_4. The amplified photocurrent implying reduced recombination and quicker photogenerated electron-hole migration on CdO/exfoliated g-C_3N_4, attributable by surface interactions between CdO and exfoliated g-C_3N_4. In comparison to exfoliated g-C_3N_4, a slight decline of the photocurrent in CdO/exfoliated g-C_3N_4 might be due to passivation of the surface by oxide layers during the reaction [49].

Photoreforming activity evaluation

Although huge efforts were taken and obtained promising results for water splitting reactions by numerous researches, the ability to produce hydrogen is still incompetent. Based on the thermodynamic point of view, hydrogen production by water splitting is a demanding process which needs higher Gibbs free energy (ΔG = +237 kJ/mol, 1.23 eV) [50]. Meanwhile, photoreforming of organic compounds tend to be less endergonic that reduces the backward reaction of O_2 while providing more viable route for H_2 generation [51]. Various precious noble metal nanoparticles especially Pt, Au and Pd were employed as dopants in the photoreforming reactions owing to their properties of acting as active sites for alcohol dehydrogenation or decarbonylation [50]. Naldoni et al., investigated the photoreforming of methanol by Pt and Au doped TiO_2 where the metals were act as electron sink and lower the recombination of e^-/h^+ pairs by creating the Schottky barrier's that will consequently results in greater hydrogen generation rate of 15 800 μmol$g^{-1}h^{-1}$ (Au-TiO_2). The study also pointed out that presence of noble metal on TiO_2 surface giving rise to surface sites ensuring more effective adsorption and oxidation of organic species participate in the reaction [52]. Chung et al., prepared Pt modified TiO_2 through one-pot synthesis approach that was subjected to

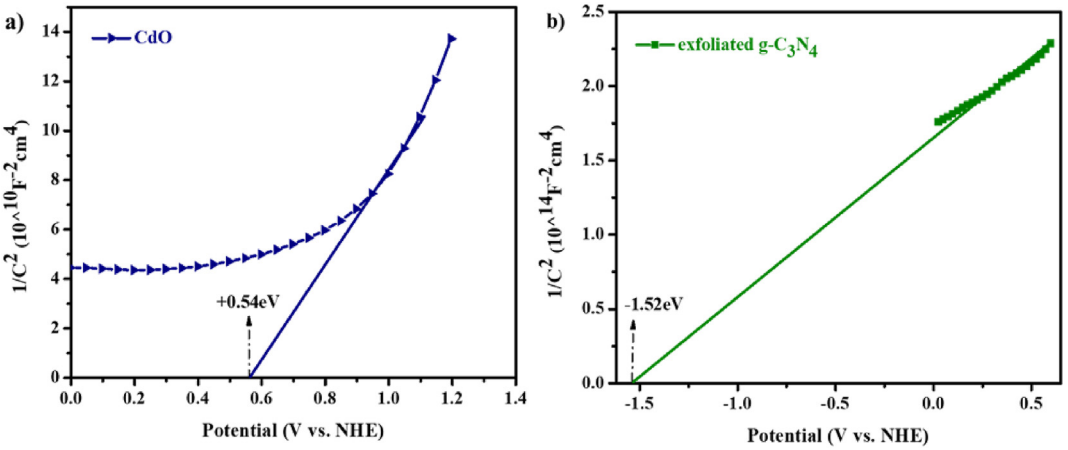

Fig. 5 − Mott-Schottky plot in 0.1 M $NaHCO_3$ aqueous solution under light off environment: (a) CdO and (b) exfoliated g-C_3N_4.

Please cite this article as: Munusamy TD et al., Sustainable hydrogen production by CdO/exfoliated g-C_3N_4 via photoreforming of formaldehyde containing wastewater, International Journal of Hydrogen Energy, https://doi.org/10.1016/j.ijhydene.2021.01.176

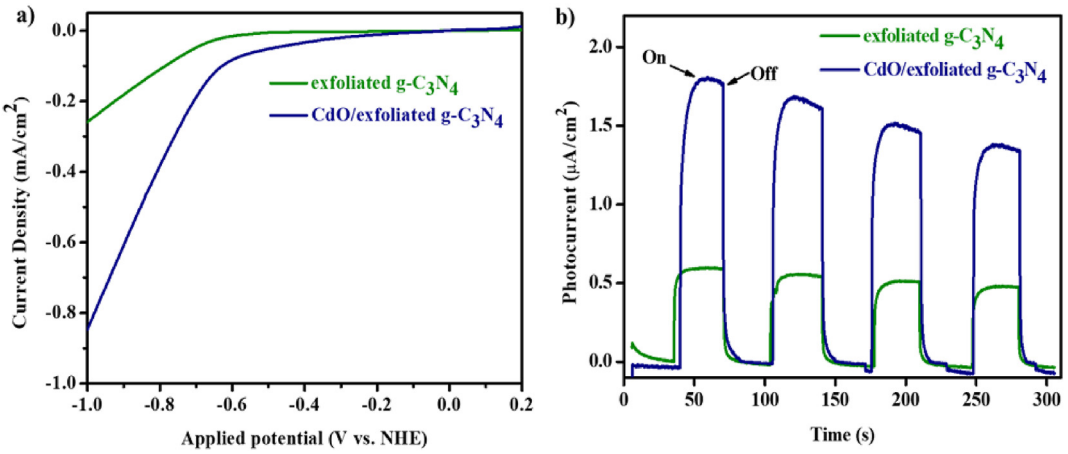

Fig. 6 – (a) LSV polarization curves of exfoliated g-C_3N_4 and CdO/exfoliated g-C_3N_4, (b) Chronoamperometry plots of exfoliated g-C_3N_4 and CdO/exfoliated g-C_3N_4. [Note: Aqueous solution of 0.1 M $NaHCO_3$ as an electrolyte].

photoreforming of methanol under 365 nm LED light illumination where the author stressed on the preparation method and compared with the conventional photodeposition of Pt technique towards the performance of hydrogen production [53]. Nevertheless, findings from the previous study on the usage of noble metals indicates that oxygen vacay induced CO generation derived from formic acid during photoreforming of methanol eventually results in Pt poisoning [54]. Moreover, Pt encapsulation by virtue of strong metal support interactions also causes rapid deactivation of the photocatalysts [55]. There are tremendous efforts to find noble metal free catalyst especially to be active in visible light. Accordingly, current research highlighted the capability of synthesised photocatalysts that can generate hydrogen without insertion of noble metal co-catalyst. The photoreforming performance of the formulated catalysts were assessed by irradiated with stimulated visible light through a cut-off filter ($\lambda > 400$ nm). Control experiments were conducted and remark was made that negligible hydrogen was evolved in the dark as well as light illumination with the absence of photocatalyst. Fig. 7(a) relates the amount of H_2 evolution from pure water and aqueous formaldehyde by various photocatalysts for a duration of 8 h. As for CdO, the hydrogen production from pure water was the least which is only 5 $\mu molg^{-1}$. The limited activity of CdO for water splitting was caused by rapid recombination between photogenerated electron and holes meanwhile the introduction of stable nanosheets, exfoliated g-C_3N_4 accelerates the hydrogen efficiency up to 94% on the CdO/exfoliated g-C_3N_4. Shi et al., reported the similar reaction using CdS and the authors found that there was negligible hydrogen produced nevertheless, when certain amount of co-catalyst, CoP was added the hydrogen generation was significantly accelerated to 231 $\mu molg^{-1}h^{-1}$ [56]. In this context, the direct photosplitting of water has thermodynamic and kinetic challenges which can be overcome by the addition of oxygenated organic substrates or sacrificial agents, that behave as water reductants. Subsequently, under anaerobic conditions, this process was referred as photoreforming (PR). Past few decades, a broad range of sacrificial reagents have been reported in literatures including methanol, ethanol, glycerol, triethanolamine, EDTA and etc. which are attractive sources of hydrogen [57]. According to Bowker et al., the sacrificial agents with hydrogen atoms in the α-position with respect to hydroxyl group proved to be effective for H_2 production since OH groups capture the photogenerated h^+, thus mitigating the e^-/h^+ recombination. However, the main drawback of these compounds is nonrenewable attributes. Thereby, hydrogen production from wastewaters serve as dual role that is production of valuable fuel as well as wastewater treatment. In this research, aqueous formaldehyde (FA) of 100 mg/L which replicate the synthetic wastewater was investigated. It was found that the hydrogen production was very significant which was 58 and 87 $\mu molg^{-1}$ for the bulk gCN and exfoliated g-C_3N_4 respectively. Meanwhile, the enhanced hydrogen production rate in exfoliated g-C_3N_4 was majorly owing to large surface area of the nanosheets offering great extent of active sites for the reaction to occur. The CdO/exfoliated g-C_3N_4 exhibited hydrogen production rate of 145 $\mu molg^{-1}$ which was approximately 7-fold higher than the pure CdO. The increase in hydrogen evolution was due to scavenging of photogenerated holes causes inhibition of recombination rate of charge carriers thereby producing more hydrogen. Besides, the solar-to-hydrogen (STH) conversion efficiency was calculated based on the following equation [58]. Basically, STH defined the ratio of Gibbs free energy stored in hydrogen molecule to the energy of sunlight consumed to generate hydrogen.

$$STH\ (\%) = \frac{rH_2\left(\frac{mol}{s}\right) \times \Delta G\left(\frac{kJ}{mol}\right)}{Solar\ flux\left(\frac{W}{m^2}\right) \times Reactor\ surface\ area\ (m^2)} \quad (6)$$

where rH_2 represents the rate of hydrogen production and ΔG is 237 kJ/mol. Hence, the STH (%) for CdO/exfoliated g-C_3N_4 was calculated to be 2.69% under light irradiation. The value obtained was comparable with literatures and Mehta et al. [59] studied water splitting reaction for hydrogen production using carbon materials such as carbon quantum dots (CQDs) and Au-CQDs where the STH efficiencies were found to be 1.75% and 1.89% respectively.

Please cite this article as: Munusamy TD et al., Sustainable hydrogen production by CdO/exfoliated g-C_3N_4 via photoreforming of formaldehyde containing wastewater, International Journal of Hydrogen Energy, https://doi.org/10.1016/j.ijhydene.2021.01.176

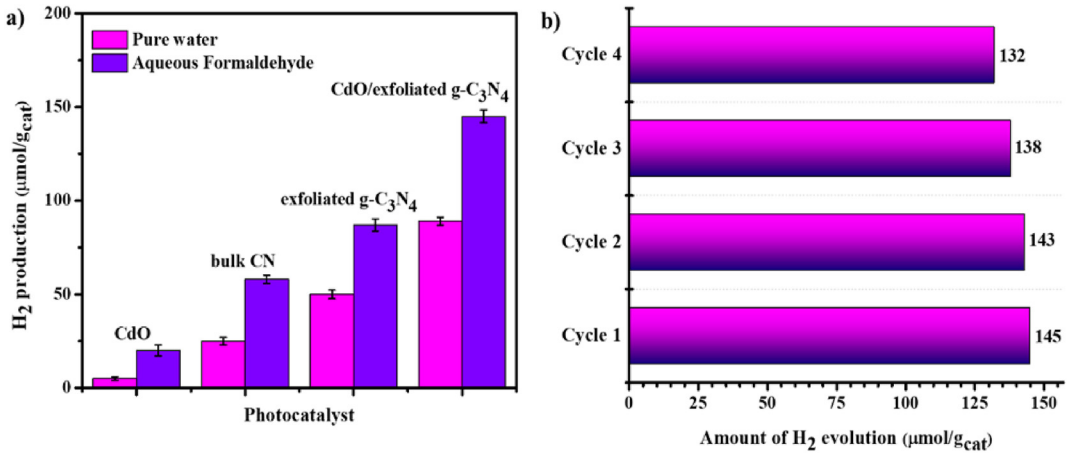

Fig. 7 – (a) Comparison of H_2 production from pure water and aqueous formaldehyde, (b) Photoreforming recycling performance of CdO/exfoliated g-C_3N_4 [Reaction conditions: Aqueous formaldehyde (100 mg/L), 0.5 g/L of catalyst].

The reusability test of the CdO/exfoliated g-C_3N_4 was investigated by conducting the photoreforming experiment of aqueous formaldehyde repeated for four times, total duration of 32 h comprising 8 h in each cycle. After every test, the catalyst was washed with water and dried at 65 °C prior to the following cycle. Based on Fig. 7(b), the first and second revealed a stable hydrogen production of 145 and 143 $\mu molg^{-1}$ respectively. Despite that, a slight decrease in the hydrogen production was detected for the last two cycles which could attribute to the loss of catalyst during the recover process [60].

Photoreforming reaction mechanism

The hydrogen evolution of photoreforming of aqueous formaldehyde was significantly increased when tested with CdO/exfoliated g-C_3N_4 nanocomposite. The synergetic effects of coupling a wide band gap semiconductor, exfoliated g-C_3N_4 nanosheets with a narrow band gap, CdO was extensively explained. As per band gap and band positions, the catalysts could absorb the light energy (especially the visible region) and produced the e^-/h^+ pairs. Due to suitable band alignment of CdO, it was thermodynamically reasonable to migrate the photoexcited e^- from the CB of CdO to the VB of exfoliated g-C_3N_4 which may function as oxidation site. The photo excited e^- of exfoliated g-C_3N_4 at its CB position functioned as reduction site. Thus, it can be inferred that the mechanism followed a Z-Scheme reaction pathway as presented in Scheme 1. The possible reactions are expressed in the following equations [61]:

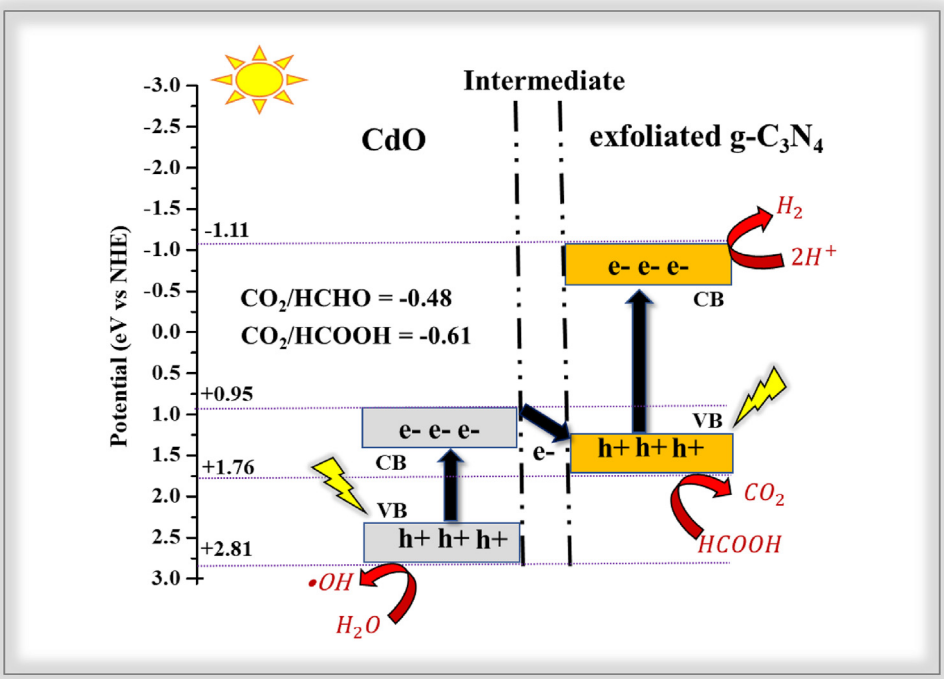

Scheme 1 – Possible Z-Scheme reaction mechanism of CdO/exfoliated g-C_3N_4 nanocomposite.

Please cite this article as: Munusamy TD et al., Sustainable hydrogen production by CdO/exfoliated g-C_3N_4 via photoreforming of formaldehyde containing wastewater, International Journal of Hydrogen Energy, https://doi.org/10.1016/j.ijhydene.2021.01.176

$$CdO/g-C_3N_4 + h\nu \rightarrow e^- + h^+ \quad (7)$$

$$H_2O + h^+ \rightarrow \bullet OH + H^+ \quad (8)$$

$$HCHO + \bullet OH \rightarrow HCOOH + H\bullet \quad (9)$$

$$HCOOH + 2h^+ \rightarrow CO_2 + 2H^+ \quad (10)$$

$$2H^+ + 2e^- \rightarrow H_2 \quad (11)$$

It is well reported in literature that the alcohols, aldehyde and organic acids function as electron donor during photocatalytic reactions in aqueous phase. It can be deduced that the more negative CB of exfoliated g-C_3N_4 (−1.11 V vs. NHE) are well-matched for the photocatalytic hydrogen production [$E(H^+/H_2)$ = −0.41 V vs. NHE] by reducing the H^+ [9,62]. Meanwhile, at the valence bands of both CdO (+2.81 V vs. NHE) and exfoliated g-C_3N_4 (+1.76 V vs. NHE), the reactions were initiated by stepwise oxidation of formaldehyde into formic acid that will finally decompose into carbon dioxide. As an initial step in Eq. (7), when the light was illuminated, electrons were promoted from VB to CB, creating an electronic vacay. The valence band sites of the catalyst are more potent to oxidize the water adsorbed on the catalyst surface forming the hydroxyl radical (•OH) as illustrated in Eq. (8) [63,64]. Belhadj et al., demonstrated that •OD radicals could be formed under UV- light illumination over Pt/TiO_2 catalyst when D_2O along with water was used as solvent. The authors also revealed the role of photocatalyst during formaldehyde oxidation with simultaneous production of H_2. It was found that D_2O and H_2O acted as electron donor at the photogenerated holes. The •OH can further oxidize formaldehyde to formic acid (Eq. (9)). The authors also proposed that oxidation of formaldehyde was majorly occurred directly by •OD radicals producing deuterated formic acid as an intermediate [25]. Thereafter, the formic acid can further be oxidized in the valance band position of the catalyst. Finally, the H^+ derived from Eqs. (8) and (10) can be reduced in the conduction band position of exfoliated g-C_3N_4 leading to generation of hydrogen (Eq. (11)) Hence, photoreforming of FA clearly possessed numerous benefits since the H^+ contributed by the oxidation reactions were also participated in the reduction reaction and subsequently enhanced the overall hydrogen production rate.

Conclusions

The CdO/exfoliated g-C_3N_4 was successfully formulated by hydrothermal approach. The current work assured that the inclusion of CdO as a co-catalyst could significantly reduce the band gap of the exfoliated g-C_3N_4 nanosheets causing inhibition of recombination rate of charge carriers. The modifications also permit uniform attachment of CdO nanoparticles which responsible for the reduction of intensity that can be inferred from the TEM and PL findings. Moreover, chronoamperometry test revealed an excellent property of CdO/exfoliated g-C_3N_4 which contained 3-fold larger photocurrent than the exfoliated g-C_3N_4 nanosheets. The photocatalytic activity of CdO/exfoliated g-C_3N_4 in both pure water and synthetic wastewater (aqueous formaldehyde) using were superior than the pure CdO, bulk gCN and exfoliated g-C_3N_4. A higher amount of hydrogen was generated (145 $\mu molg^{-1}$) when synthetic wastewater comprising with 100 mg/L of formaldehyde was used. The plausible mechanism for photoreforming of formaldehyde over CdO/exfoliated g-C_3N_4 catalyst has been proposed. Hence, this study is significant where it provides a new insight to the design of effective Z-Scheme visible light active catalyst for the photoreforming of FA containing wastewater to produce hydrogen.

Declaration of competing interest

The authors declare that they have no known competing financial interests or personal relationships that could have appeared to influence the work reported in this paper.

Acknowledgment

The current research was funded by Ministry of Higher Education, Malaysia under Trans-disciplinary Grant Scheme RDU191802-1 (TRGS/1/2018/UMP/02/2/1). The authors are also appreciate Universiti Malaysia Pahang for the facilities provided.

Appendix A. Supplementary data

Supplementary data to this article can be found online at https://doi.org/10.1016/j.ijhydene.2021.01.176.

REFERENCES

[1] IEA (International Energy Agency). The future of hydrogen. Paris: IEA; 2019. https://www.iea.org/reports/the-future-of-hydrogen.
[2] Uekert T, Dorchies F, Pichler CM, Reisner E. Photoreforming of food waste into value-added products over visible-light-absorbing catalysts. Green Chem 2020;22:3262–71.
[3] Li X, Yan B, Zhang J, Xu N, Tao J, Zhang R, Liu B, Sun Z, Chen G. Hydrogen production by aqueous phase reforming of phenol derived from lignin pyrolysis over NiCe/ZSM-5 catalysts. Int J Hydrogen Energy 2018;43:649–58.
[4] Chowdhury P, Malekshoar G, Ray MB, Zhu J, Ray AK. Sacrificial hydrogen generation from formaldehyde with Pt/TiO_2 photocatalyst in solar radiation. Ind Eng Chem Res 2013;52:5023–9.
[5] Yeruva DK, Jukuri S, Velvizhi G, Naresh Kumar A, Swamy YV, Venkata Mohan S. Integrating sequencing batch reactor with bio-electrochemical treatment for augmenting remediation efficiency of complex petrochemical wastewater. Bioresour Technol 2015;188:33–42.
[6] Tian X, Song Y, Shen Z, Zhou Y, Wang K, Jin X, Han Z, Liu T. A comprehensive review on toxic petrochemical wastewater pretreatment and advanced treatment. J Clean Prod 2020;245:118692.
[7] Mei X, Guo Z, Liu J, Bi S, Li P, Wang Y, Shen W, Yang Y, Wang Y, Xiao Y, Yang X, Liu Y, Zhao L, Wang Y, Hu S.

Treatment of formaldehyde wastewater by a membrane-aerated biofilm reactor (MABR): the degradation of formaldehyde in the presence of the cosubstrate methanol. Chem Eng J 2019;372:673–83.
[8] IARC, IARC Classifies Formaldehyde as Carcinogenic. Oncol Times 2004;26:72.
[9] Liu J, Fang W, Wei Z, Qin Z, Jiang Z, Shangguan W. Efficient photocatalytic hydrogen evolution on N-deficient g-C_3N_4 achieved by a molten salt post-treatment approach. Appl Catal B Environ 2018;238:465–70.
[10] Hao X, Zhou J, Cui Z, Wang Y, Wang Y, Zou Z. Zn-vacancy mediated electron-hole separation in ZnS/g-C_3N_4 heterojunction for efficient visible-light photocatalytic hydrogen production. Appl Catal B Environ 2018;229:41–51.
[11] Wu X, Cheng J, Li X, Li Y, Lv K. Enhanced visible photocatalytic oxidation of NO by repeated calcination of g-C_3N_4. Appl Surf Sci 2019;465:1037–46.
[12] Guo S, Tang Y, Xie Y, Tian C, Feng Q, Zhou W, Jiang B. P-doped tubular g-C_3N_4 with surface carbon defects: universal synthesis and enhanced visible-light photocatalytic hydrogen production. Appl Catal B Environ 2017;218:664–71.
[13] Li Y, Yang M, Xing Y, Liu X, Yang Y, Wang X, Song S. Preparation of carbon-rich g-C_3N_4 nanosheets with enhanced visible light utilization for efficient photocatalytic hydrogen production. Small 2017;13:1701552.
[14] Sun S, Li J, Cui J, Gou X, Yang Q, Jiang Y, Liang S, Yang Z. Simultaneously engineering K-doping and exfoliation into graphitic carbon nitride (g-C_3N_4) for enhanced photocatalytic hydrogen production. Int J Hydrogen Energy 2019;44:778–87.
[15] Liu Q, Shen J, Yu X, Yang X, Liu W, Yang J, Tang H, Xu H, Li H, Li Y, Xu J. Unveiling the origin of boosted photocatalytic hydrogen evolution in simultaneously (S, P, O)-Codoped and exfoliated ultrathin g-C3N4 nanosheets. Appl Catal B Environ 2019;248:84–94.
[16] Yuan Y-J, Shen Z, Wu S, Su Y, Pei L, Ji Z, et al. Liquid exfoliation of g-C_3N_4 nanosheets to construct 2D-2D MoS_2/g-C_3N_4 photocatalyst for enhanced photocatalytic H_2 production activity. Appl Catal B Environ 2019;246:120–8.
[17] Niu Ping, Zhang L, Liu G, Cheng H-M. Graphene-like carbon nitride nanosheets for improved photocatalytic activities. Adv Funct Mater 2012;22:4763–70.
[18] Masudy-Panah S, Siavash Moakhar R, Chua CS, Kushwaha A, Dalapati GK. Stable and efficient CuO based photocathode through oxygen-rich composition and Au–Pd nanostructure incorporation for solar-hydrogen production. ACS Appl Mater Interfaces 2017;9:27596–606.
[19] Saadetnejad D, Yıldırım R. Photocatalytic hydrogen production by water splitting over Au/Al-SrTiO3. Int J Hydrogen Energy 2018;43:1116–22.
[20] Luo Z, Wang Z, Li J, Yang K, Zhou G. N-Promoted Ru 1/TiO_2 single-atom catalysts for photocatalytic water splitting for hydrogen production: a density functional theory study. Phys Chem Chem Phys 2020;22:11392–9.
[21] Tong J, Li C, Bo L, Guan X, Wang Y, Kong D, et al. Bimetallic Fe–Co chalcogenophosphates as highly efficient bifunctional electrocatalysts for overall water splitting. Int J Hydrogen Energy 2020;46(5):3354–64.
[22] Kurenkova AY, Markovskaya DV, Gerasimov EY, Prosvirin IP, Cherepanova SV, Kozlova EA. New insights into the mechanism of photocatalytic hydrogen evolution from aqueous solutions of saccharides over CdS-based photocatalysts under visible light. Int J Hydrogen Energy 2020;45:30165–77.
[23] Kumar PS, Selvakumar M, Bhagabati P, Bharathi B, Karuthapandian S, Balakumar S. CdO/ZnO nanohybrids: facile synthesis and morphologically enhanced photocatalytic performance. RSC Adv 2014;4:32977.
[24] Munawar T, Iqbal F, Yasmeen S, Mahmood K, Hussain A. Multi metal oxide NiO-CdO-ZnO nanocomposite–synthesis, structural, optical, electrical properties and enhanced sunlight driven photocatalytic activity. Ceram Int 2020;46:2421–37.
[25] Belhadj H, Hamid S, Robertson PKJ, Bahnemann DW. Mechanisms of simultaneous hydrogen production and formaldehyde oxidation in H_2O and D_2O over platinized TiO_2. ACS Catal 2017;7:4753–8.
[26] Munusamy TD, Yee CS, Khan MMR. Construction of hybrid g-C_3N_4/CdO nanocomposite with improved photodegradation activity of RhB dye under visible light irradiation. Adv Powder Technol 2020;31(7):2921–31.
[27] Papailias I, Todorova N, Giannakopoulou T, Ioannidis N, Boukos N, Athanasekou CP, Dimotikali D, Trapalis C. Chemical vs thermal exfoliation of g-C_3N_4 for NOx removal under visible light irradiation. Appl Catal B Environ 2018;239:16–26.
[28] Kumar S, Ahmed B, Ojha AK, Das J, Kumar A. Facile synthesis of CdO nanorods and exploiting its properties towards supercapacitor electrode materials and low power UV irradiation driven photocatalysis against methylene blue dye. Mater Res Bull 2017;90:224–31.
[29] Deng S, Yang Z, Lv G, Zhu Y, Li H, Wang F, Zhang X. WO_3 nanosheets/g-C_3N_4 nanosheets' nanocomposite as an effective photocatalyst for degradation of rhodamine B. Appl Phys A 2019;125:44.
[30] Rezaul Karim KM, Tarek M, Ong HR, Abdullah H, Yousuf A, Cheng CK, Khan MMR. Photoelectrocatalytic reduction of carbon dioxide to methanol using $CuFe_2O_4$ modified with graphene oxide under visible light irradiation. Ind Eng Chem Res 2019;58:563–72.
[31] Zhao Z, Zhang X, Fan J, Xue D, Zhang B, Yin S. N-TiO_2/g-C_3N_4/Up-conversion phosphor composites for the full-spectrum light-responsive deNOx photocatalysis. J Mater Sci 2018;53:7266–78.
[32] Wu M, Gong Y, Nie T, Zhang J, Wang R, Wang H, He B. Template-free synthesis of nanocage-like g-C_3N_4 with high surface area and nitrogen defects for enhanced photocatalytic H 2 activity. J Mater Chem A 2019;7:5324–32.
[33] Zhang W, Xiao X, Li Y, Zeng X, Zheng L, Wan C. Liquid-exfoliation of layered MoS_2 for enhancing photocatalytic activity of TiO_2/g-C_3N_4 photocatalyst and DFT study. Appl Surf Sci 2016;389:496–506.
[34] Hang NT, Zhang S, Yang W. Efficient exfoliation of g-C_3N_4 and NO_2 sensing behavior of graphene/g-C_3N_4 nanocomposite. Sensor Actuator B Chem 2017;248:940–8.
[35] Thomas P, Sreekanth P, Philip R, Abraham KE. Morphology dependent nanosecond and ultrafast optical power limiting of CdO nanomorphotypes. RSC Adv 2015;5:35017–25.
[36] Dong F, Li Y, Wang Z, Ho W-KK. Enhanced visible light photocatalytic activity and oxidation ability of porous graphene-like g-C_3N_4 nanosheets via thermal exfoliation. Appl Surf Sci 2015;358:393–403.
[37] Zhou P, Le Z, Xie Y, Fang J, Xu J. Studies on facile synthesis and properties of mesoporous CdS/TiO_2 composite for photocatalysis applications. J Alloys Compd 2017;692:170–7.
[38] Anitha S, Suganya M, Prabha D, Srivind J, Balamurugan S, Balu AR. Synthesis and characterization of NiO-CdO composite materials towards photoconductive and antibacterial applications. Mater Chem Phys 2018;211:88–96.
[39] Liang S, Zhang D, Pu X, Yao X, Han R, Yin J, Ren X. A novel Ag_2O/g-C_3N_4 p-n heterojunction photocatalysts with enhanced visible and near-infrared light activity. Separ Purif Technol 2019;210:786–97.
[40] Mohamed NA, Safaei J, Ismail AF, Mohamad Noh MF, Arzaee NA, Mansor NN, Ibrahim MA, Ludin NA, Sagu JS, Mat Teridi MA. Fabrication of exfoliated graphitic carbon nitride,

Please cite this article as: Munusamy TD et al., Sustainable hydrogen production by CdO/exfoliated g-C_3N_4 via photoreforming of formaldehyde containing wastewater, International Journal of Hydrogen Energy, https://doi.org/10.1016/j.ijhydene.2021.01.176

($g\text{-}C_3N_4$) thin film by methanolic dispersion. J Alloys Compd 2020;818:152916.
[41] Bao N, Hu X, Zhang Q, Miao X, Jie X, Zhou S. Synthesis of porous carbon-doped $g\text{-}C_3N_4$ nanosheets with enhanced visible-light photocatalytic activity. Appl Surf Sci 2017;403:682–90.
[42] Tian W, Li N, Zhou J. A novel P-doped $g\text{-}C_3N_4/Zn_{0.8}Cd_{0.2}S$ composite photocatalyst for degradation of methylene blue under simulated sunlight. Appl Surf Sci 2016;361:251–8.
[43] Tan X, Wang X, Hang H, Zhang D, Zhang N, Xiao Z, Tao H. Self-assembly method assisted synthesis of $g\text{-}C_3N_4$/ZnO heterostructure nanocomposites with enhanced photocatalytic performance. Opt Mater (Amst) 2019;96:109266.
[44] Fu J, Xu Q, Low J, Jiang C, Yu J. Ultrathin 2D/2D $WO_3/g\text{-}C_3N_4$ step-scheme H_2-production photocatalyst. Appl Catal B Environ 2019;243:556–65.
[45] Cao S, Shen B, Tong T, Fu J, Yu J. 2D/2D heterojunction of ultrathin MXene/Bi_2 WO_6 nanosheets for improved photocatalytic CO_2 reduction. Adv Funct Mater 2018;28:1800136.
[46] Giannakopoulou T, Papailias I, Todorova N, Boukos N, Liu Y, Yu J, Trapalis C. Tailoring the energy band gap and edges' potentials of $g\text{-}C_3N_4/TiO_2$ composite photocatalysts for NOxremoval. Chem Eng J 2017;310:571–80.
[47] Saravanakumar K, Muthupoongodi S, Muthuraj V. A novel n-CeO_2/n-CdO heterojunction nanocomposite for enhanced photodegradation of organic pollutants under visible light irradiation. J Rare Earths 2019;37:853–60.
[48] Cheng C, Zong S, Shi J, Xue F, Zhang Y, Guan X, Zheng B, Deng J, Guo L. Facile preparation of nanosized MoP as cocatalyst coupled with $g\text{-}C_3N_4$ by surface bonding state for enhanced photocatalytic hydrogen production. Appl Catal B Environ 2020;265:118620.
[49] Yi Y, Weinberg G, Prenzel M, Greiner M, Heumann S, Becker S, Schlögl R. Electrochemical corrosion of a glassy carbon electrode. Catal Today 2017;295:32–40.
[50] Rossetti I. Hydrogen production by photoreforming of renewable substrates. ISRN Chem Eng 2012;2012:1–21.
[51] Wang C, Bu E, Chen Y, Cheng Z, Zhang J, Shu R, Song Q. Enhanced photoreforming hydrogen production: pickering interfacial catalysis from a bio-derived biphasic system. Renew Energy 2019;134:113–24.
[52] Naldoni A, D'Arienzo M, Altomare M, Marelli M, Scotti R, Morazzoni F, Selli E, Dal Santo V. Pt and Au/TiO_2 photocatalysts for methanol reforming: role of metal nanoparticles in tuning charge trapping properties and photoefficiency. Appl Catal B Environ 2013;130–131:239–48.
[53] Chung Y-H, Han K, Lin C-Y, O'Neill D, Mul G, Mei B, Yang C-M. Photocatalytic hydrogen production by photo-reforming of methanol with one-pot synthesized Pt-containing TiO_2 photocatalysts. Catal Today 2020;356:95–100.
[54] Chiarello GL, Aguirre MH, Selli E. Hydrogen production by photocatalytic steam reforming of methanol on noble metal-modified TiO_2. J Catal 2010;273:182–90.
[55] Haselmann GM, Eder D. Early-stage deactivation of platinum-loaded TiO_2 using in situ photodeposition during photocatalytic hydrogen evolution. ACS Catal 2017;7:4668–75.
[56] Shi R, Ye H-F, Liang F, Wang Z, Li K, Weng Y, Lin Z, Fu W-F, Che C-M, Chen Y. Interstitial P-doped CdS with long-lived photogenerated electrons for photocatalytic water splitting without sacrificial agents. Adv Mater 2018;30:1705941.
[57] Zhu R, Tian F, Yang R, He J, Zhong J, Chen B. Z scheme system $ZnIn_2S_4$/RGO/$BiVO_4$ for hydrogen generation from water splitting and simultaneous degradation of organic pollutants under visible light. Renew Energy 2019;139:22–7.
[58] Varadhan P, Fu H-C, Kao Y-C, Horng R-H, He J-H. An efficient and stable photoelectrochemical system with 9% solar-to-hydrogen conversion efficiency via InGaP/GaAs double junction. Nat Commun 2019;10:5282.
[59] Mehta A, D. P, Thakur A, Basu S. Enhanced photocatalytic water splitting by gold carbon dot core shell nanocatalyst under visible/sunlight. New J Chem 2017;41:4573–81.
[60] Ranjith KS, Rajendra Kumar RT. Regeneration of an efficient, solar active hierarchical ZnO flower photocatalyst for repeatable usage: controlled desorption of poisoned species from active catalytic sites. RSC Adv 2017;7:4983–92.
[61] Christoforidis KC, Fornasiero P. Photocatalytic hydrogen production: a rift into the future energy supply. ChemCatChem 2017;9:1523–44.
[62] Sanwald KE, Berto TF, Eisenreich W, Gutiérrez OY, Lercher JA. Catalytic routes and oxidation mechanisms in photoreforming of polyols. J Catal 2016;344:806–16.
[63] Siahrostami S, Li G-L, Viswanathan V, Nørskov JK. One- or two-electron water oxidation, hydroxyl radical, or H_2O_2 evolution. J Phys Chem Lett 2017;8:1157–60.
[64] Kesselman JM, Weres O, Lewis NS, Hoffmann MR. Electrochemical production of hydroxyl radical at polycrystalline Nb-doped TiO_2 electrodes and estimation of the partitioning between hydroxyl radical and direct hole oxidation pathways. J Phys Chem B 1997;101:2637–43.

Please cite this article as: Munusamy TD et al., Sustainable hydrogen production by CdO/exfoliated $g\text{-}C_3N_4$ via photoreforming of formaldehyde containing wastewater, International Journal of Hydrogen Energy, https://doi.org/10.1016/j.ijhydene.2021.01.176